THE JOURNAL OF PHYSICAL CHEMISTRY B
A JOURNAL OF THE AMERICAN CHEMICAL SOCIETY

pubs.acs.org/JPCB

Article

Orientational Pair Correlations and Local Structure of Benzonitrile from Molecular Dynamics Simulations with Comparisons to Experiments

Maolin Sha,[§] Steven A. Yamada,[§] and Michael D. Fayer*

Cite This: *J. Phys. Chem. B* 2021, 125, 3163–3177

Read Online

ACCESS | Metrics & More | Article Recommendations | Supporting Information

ABSTRACT: We present an experimentally parametrized molecular dynamics study of single-molecule and collective orientational relaxation in neat benzonitrile through the analysis of the reorientational anisotropy and polarizability anisotropy time correlation function (PA-TCF). The simulations show that the PA-TCF is dominated by collective reorientation after 20 ps. Collective reorientation is found to be slower than single-molecule reorientation by a factor of 1.67, consistent with recent experiments. The simulations provide direct evidence of local antiparallel benzonitrile configurations. These structures, which have been the center of some debate, are responsible for the slower rate of collective versus single-molecule reorientation in the liquid. Further structural analysis indicates that significant Coulombic interactions between the nitrile group and hydrogen atoms on adjacent molecules play a role in the formation of the antiparallel structures. The single-molecule dynamics reflected in the anisotropy are complex and consist of a ballistic regime, restricted angular diffusion, and spatially anisotropic free diffusion. The principal components of the rotational diffusion tensor are independently obtained and shown to reproduce the free diffusion regime of the anisotropy for each principal axis according to the predictions of a previous theory.

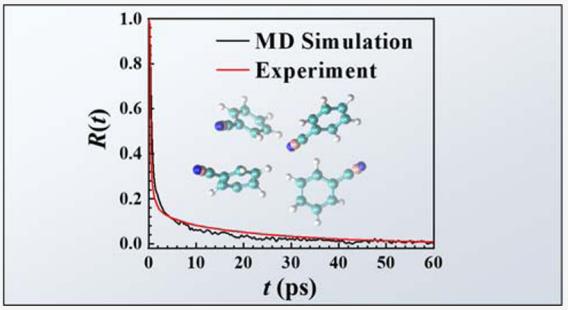

1. INTRODUCTION

Over the last few decades, third-order optical and infrared (IR) spectroscopies have emerged as indispensable techniques for advancing our understanding of liquid dynamics and the motions and interactions that underlie them.[1,2] The use of these methods has elucidated a range of processes occurring on femtosecond to picosecond time scales, including molecular reorientation,[3,4] collision-induced effects,[5] homogeneous and inhomogeneous dephasing,[1,2] and chemical exchange.[6] To date, a wide variety of liquids with properties spanning nonpolar to polar, ionic to H-bonding, and super-cooled to glasses have been investigated.[7−13]

Still, even in the case of ordinary liquids, it can be very challenging to determine the time scales and contributions of different molecular motions to a measured signal.[8] In many cases, the interdependence between dynamics and mesoscopic liquid structures adds complexity to the interpretation of experiments.[14] Molecular dynamics (MD) simulations have proven useful in this regard because they allow any suitably defined motion or interaction to be investigated with arbitrary resolution. Simulations can be vetted by comparison with measured properties, and then can provide microscopic insights into the validity of experimental assumptions and the predictions of liquid theories.

In this work, we present an experimentally parametrized MD simulation study of the single-molecule and collective reorientation dynamics of liquid benzonitrile. In a previous study,[14] the former was measured with IR polarization-selective pump−probe (PSPP) experiments and the later with optical Kerr effect (OKE) spectroscopy, the time-domain analogue of depolarized Rayleigh scattering (DRS).[15] Both methods are pump−probe techniques that use two input pulses of linearly polarized light to measure the third-order material response of a liquid sample.[3,4,16,17]

In the PSPP (transient absorption) experiment, the incident pulses are resonant with a dipole transition associated with a molecular vibration,[1−3] in this case, the CN stretching mode of benzonitrile. The acquired signal is the transient absorption of a time-delayed probe pulse following excitation of the sample by a pump pulse.[4] The signals obtained using mutually parallel or perpendicular pulse polarizations measure separate tensor elements of the single-molecule orientational response function.[2,3] The signals can be appropriately combined to obtain the reorientational anisotropy, or equivalently, the orientational correlation function, which contains information

Received: December 14, 2020
Revised: February 24, 2021
Published: March 17, 2021

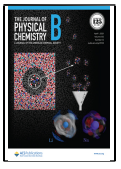

https://doi.org/10.1021/acs.jpcb.0c11148
J. Phys. Chem. B 2021, 125, 3163−3177

on the single-molecule rotational dynamics.[3,4,18] Note that "single-molecule" is used here to mean that the orientational correlation function is the ensemble-average of the rotational dynamics of single molecules.

In OKE (transient birefringence) spectroscopy, the optical pulses have the same frequency but are not resonant with any electronic or vibrational transition in the liquid.[8,16,17] Through a Raman excitation process, the pump exerts a torque on the optically anisotropic molecules in the sample.[19] In response, the molecules minutely reorient in a way that slightly aligns the long axis of their polarizability tensor parallel to the polarization of the pump, making the refractive index (susceptibility) parallel and perpendicular to the pump polarization different (birefringence).[16,17,19] The time-delayed probe pulse, linearly polarized at 45° relative to the pump polarization, passes through the sample, and acquires an additional component orthogonal to its original polarization direction, making it elliptically polarized. This transient, pump-induced polarization component in the probe pulse is the third-order OKE signal field.[17] Throughout this paper, OKE refers to the heterodyne-detected version of this experiment, in which the measured signal is linear in the emitted field and third-order material response.[5,8,16,17]

The OKE experiment, as described above, measures the anisotropic nuclear response function, which is related to the time-derivative of the (classical) polarizability anisotropy time correlation function (PA-TCF).[1,8,17,20] The anisotropic nuclear response is strongly influenced by motions with collective reorientational character. Historically, it has been debated whether the single-molecule and collective reorientation times for benzonitrile differ.[14,21−27] In principle, collision-induced decay mechanisms can significantly influence the OKE signals of liquids for several picoseconds, and in some cases for the full extent of the decay.[28,29] Therefore, OKE experiments must invoke a separation of time scales to analyze collective reorientation separately from collision-induced effects, an issue that is not encountered with the single-molecule anisotropy from PSPP experiments.

To further address these issues, we analyze the reorientational anisotropy and OKE signals calculated from a classical molecular dynamics simulation of liquid benzonitrile. Analysis of the PA-TCF reveals that the collision-induced contribution, while important at short times, fully relaxes by 20 ps. The PA-TCF is dominated by dynamics with collective reorientational character beyond this time, justifying a key assumption from a previous experimental study.[14] The correlation time for collective reorientation is 1.67 times slower than that for single-molecule reorientation, consistent with previous experimental results.[14,22,23] Antiparallel and some parallel benzonitrile structures are directly observed in the simulation. It is shown that significant Coulombic interactions between adjacent molecules is one driving force for the formation of these aligned structures, which are responsible for the slower observed collective (relative to single-molecule) reorientation. Using rotational mean squared displacements (RMSDs), the principal components of the rotational diffusion tensor are independently obtained, and it is shown that the free-diffusion (FD) regime of the anisotropy can be quantitatively fit with these three components after accounting for wobbling-in-a-cone dynamics[30−32] at short times.

2. THEORY, COMPUTATIONAL DETAILS, AND FORCE FIELD RELIABILITY

2.1. Theoretical Background. The OKE signal reports on the time-dependent anisotropic (off-diagonal) components of the collective polarizability (second-rank) tensor of a liquid sample.[8,28,29,33−37] The collective polarizability tensor of an N molecule system can be expressed as a sum of molecular (M) and interaction-induced terms (I)

$$\boldsymbol{\Pi} = \boldsymbol{\Pi}^{\mathrm{M}} + \boldsymbol{\Pi}^{\mathrm{I}} \tag{1}$$

The molecular contribution, $\boldsymbol{\Pi}^{\mathrm{M}}$, is the sum of the individual molecular polarizabilities, $\boldsymbol{\alpha}_i$

$$\boldsymbol{\Pi}^{\mathrm{M}} = \sum_{i=1}^{N} \boldsymbol{\alpha}_i \tag{2}$$

The interaction-induced contribution, $\boldsymbol{\Pi}^{\mathrm{I}}$, arises from interactions between molecular-induced dipoles. The field of the dipole induced in one molecule by the incident pump pulse can polarize another molecule; the dipole induced in the second molecule is not, in general, parallel to the pump polarization (anisotropic).[33] The interaction-induced contribution can be calculated from the first-order dipole-induced dipole (DID) to the all-orders DID approximation, as has been performed in several previous MD simulations.[8,28,29,33,35−37] The dielectric constant (relative permittivity) of benzonitrile is about 26, which is moderately smaller than that for the common polar liquid acetonitrile (36).[38] Elola and Ladanyi found that the higher-order interaction-induced contributions were essentially negligible for acetonitrile liquid.[35] Similar to acetonitrile, the interaction-induced contribution to the collective polarizability of liquid benzonitrile can be effectively modeled using the first-order perturbative solution (DID), as will be demonstrated below by comparison to experimental OKE measurements

$$\boldsymbol{\Pi}^{\mathrm{I}} \cong \sum_{i=1}^{N} \sum_{j \neq i} \boldsymbol{\alpha}_i \cdot \mathbf{T}_{ij} \cdot \boldsymbol{\alpha}_j \tag{3}$$

where $\mathbf{T}_{ij} \equiv \mathbf{T}(\mathbf{r}_{ij})$ is the dipole interaction tensor. The dipole interaction tensor is determined by the vector $\mathbf{r}_{ij}$ connecting the center-of-mass of molecules i and j and is given by

$$\mathbf{T}(\mathbf{r}) = \frac{3\hat{\mathbf{r}}\hat{\mathbf{r}} - \mathbf{1}}{r^3} \tag{4}$$

where $\hat{\mathbf{r}} = \mathbf{r}/r$ is a unit vector in the direction of $\mathbf{r}$ and $\mathbf{1}$ is the unit tensor. This approximation, which involves a single site located at the center-of-mass of each molecule, has been referred to as the center−center approach.[36]

In the above expressions and those that follow, properties such as the polarizability tensor, $\boldsymbol{\alpha}$, or a unit vector along the CN bond, $\hat{\mathbf{u}}$, are represented in a laboratory (space-fixed) frame $L = XYZ$. However, it is often convenient to express them in a molecular (molecule-fixed) frame $m = xyz$. In the calculations, benzonitrile is treated as a rigid molecule. Therefore, $\boldsymbol{\alpha}$ and $\hat{\mathbf{u}}$ will be static when expressed in the m frame, which we choose to coincide with the principal axes of the polarizability tensor. With this choice, $\boldsymbol{\alpha}$ and $\hat{\mathbf{u}}$ can be expressed

https://doi.org/10.1021/acs.jpcb.0c11148
J. Phys. Chem. B 2021, 125, 3163−3177

$$\boldsymbol{\alpha}^m = \begin{bmatrix} \alpha_{xx} & & \\ & \alpha_{yy} & \\ & & \alpha_{zz} \end{bmatrix}$$

$$\hat{\mathbf{u}}^m = \begin{bmatrix} 0 \\ 0 \\ 1 \end{bmatrix} \tag{5}$$

where, for example, α_{xx} is the principal component of the polarizability tensor for the x direction (Figure 1a). At any

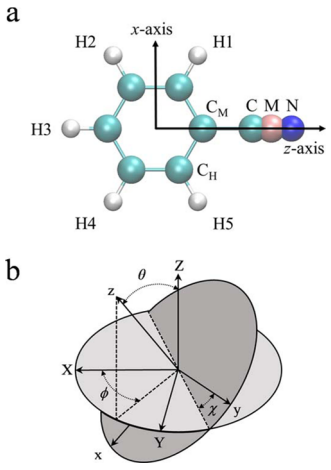

Figure 1. (a) Illustration of benzonitrile with the x and z axes of the molecular frame labeled. The mass center, M, is shown in pink. (b) Relative orientation between the molecular (xyz) and laboratory (XYZ) frames, as defined by the three Euler angles, ϕ, θ, and χ.

instant, the molecular frame will have some orientation with respect to the laboratory frame. This relative orientation is described by the three Euler angles ϕ, θ, and χ (also denoted as α, β, and γ) (Figure 1b). The transformation from the m frame to the L frame is accomplished by three successive rotations $\mathbf{R}(\chi)$, $\mathbf{R}(\theta)$, and $\mathbf{R}(\phi)$,[39]

$$\mathbf{R}(\chi, \theta, \phi) = \mathbf{R}(\phi)\mathbf{R}(\theta)\mathbf{R}(\chi)$$

$$= \begin{bmatrix} c\phi & -s\phi & 0 \\ s\phi & c\phi & 0 \\ 0 & 0 & 1 \end{bmatrix}\begin{bmatrix} c\theta & 0 & s\theta \\ 0 & 1 & 0 \\ -s\theta & 0 & c\theta \end{bmatrix}\begin{bmatrix} c\chi & -s\chi & 0 \\ s\chi & c\chi & 0 \\ 0 & 0 & 1 \end{bmatrix}$$

$$= \begin{bmatrix} c\phi c\theta c\chi - s\phi s\chi & -c\phi c\theta s\chi - s\phi c\chi & c\phi s\theta \\ s\phi c\theta c\chi + c\phi s\chi & -s\phi c\theta s\chi + c\phi c\chi & s\phi s\theta \\ -s\theta c\chi & s\theta s\chi & c\theta \end{bmatrix} \tag{6}$$

where c and s refer to the cosine and sine functions, respectively, and $\mathbf{R}(\chi,\theta,\phi)$ is the rotation matrix for the unitary transformation. Then, $\hat{\mathbf{u}}$ and $\boldsymbol{\alpha}$ are given by

$$\hat{\mathbf{u}} = \mathbf{R}\hat{\mathbf{u}}^m$$

$$\boldsymbol{\alpha} = \mathbf{R}\boldsymbol{\alpha}^m\mathbf{R}^\dagger \tag{7}$$

where $\mathbf{R}^\dagger$ is the transpose of $\mathbf{R}$ and $\mathbf{R}^\dagger = \mathbf{R}^{-1}$.[39]

The relaxation of the collective PA for liquid benzonitrile is calculated via the TCF of an off-diagonal element (such as Π_{XY}) of the collective polarizability tensor, $\boldsymbol{\Pi}$[8,28,29,33−37]

$$\psi_{XY}(t) = \frac{\langle \Pi_{XY}(0)\Pi_{XY}(t)\rangle}{\Gamma^2} \tag{8}$$

The normalization factor $\Gamma^2 = N\gamma^2/15$ in the denominator of eq 8 is the integrated intensity of the anisotropic DRS spectrum of N non-interacting molecules,[40] where $\gamma^2 = [(\alpha_{xx} - \alpha_{yy})^2 + (\alpha_{xx} - \alpha_{zz})^2 + (\alpha_{yy} - \alpha_{zz})^2]/2$ is the squared molecular PA.[28,34,35,37] By substituting eq 1 into eq 8, the PA-TCF, $\psi_{XY}(t)$, can be written as

$$\psi_{XY}(t) = \psi_{XY}^{\mathrm{MM}}(t) + \psi_{XY}^{\mathrm{MI}}(t) + \psi_{XY}^{\mathrm{II}}(t) \tag{9}$$

where

$$\psi_{XY}^{\mathrm{MM}}(t) = \langle \Pi_{XY}^{\mathrm{M}}(0)\Pi_{XY}^{\mathrm{M}}(t)\rangle/\Gamma^2,$$

$$\psi_{XY}^{\mathrm{MI}}(t) = (\langle \Pi_{XY}^{\mathrm{M}}(0)\Pi_{XY}^{\mathrm{I}}(t)\rangle + \langle \Pi_{XY}^{\mathrm{I}}(0)\Pi_{XY}^{\mathrm{M}}(t)\rangle)/\Gamma^2,$$

$$\psi_{XY}^{\mathrm{II}}(t) = \langle \Pi_{XY}^{\mathrm{I}}(0)\Pi_{XY}^{\mathrm{I}}(t)\rangle/\Gamma^2 \tag{10}$$

In eqs 9 and 10, $\psi_{XY}^{\mathrm{MM}}(t)$ and $\psi_{XY}^{\mathrm{II}}(t)$ are the molecular- and interaction-induced PA autocorrelations and $\psi_{XY}^{\mathrm{MI}}(t)$ is their cross-correlation. To improve the statistical accuracy of the correlation function, all independent off-diagonal elements (XY, XZ, and YZ) are used in eq 8 and averaged together in the calculation of $\psi(t)$.

Although the separation of $\psi(t)$ in eq 9 is straightforward, it is not necessarily the most useful because it does not distinguish between the different relaxation mechanisms, that is, collective reorientation- and collision-induced, that contribute to $\psi(t)$. Specifically, the molecular contribution, $\boldsymbol{\Pi}^{\mathrm{M}}$, is modulated by changes in molecular orientation, while the interaction-induced polarizability $\boldsymbol{\Pi}^{\mathrm{I}}$ depends on changes in the relative orientations and intermolecular distances between different molecules. Since a portion of $\boldsymbol{\Pi}^{\mathrm{I}}$ relaxes with the same mechanism as $\boldsymbol{\Pi}^{\mathrm{M}}$, there is no clear time scale separation between the different auto- and cross-correlations in eq 9. To separate the interaction-induced dynamics into a portion that has the same time-dependence as collective reorientation and a collision-induced portion that does not, we can recast $\boldsymbol{\Pi}$ in a projected representation in which $\boldsymbol{\Pi}^{\mathrm{I}}$ is projected along and orthogonal to $\boldsymbol{\Pi}^{\mathrm{M}}$[33]

$$\Pi_{XY}^{\mathrm{I}} = G_{XY}\Pi_{XY}^{\mathrm{M}} + \Pi_{XY}^{\Delta} \tag{11}$$

$$G_{XY} = \frac{\langle \Pi_{XY}^{\mathrm{M}}\Pi_{XY}^{\mathrm{I}}\rangle}{\langle |\Pi_{XY}^{\mathrm{M}}|^2\rangle} = \frac{\psi_{XY}^{\mathrm{MI}}(0)}{2\psi_{XY}^{\mathrm{MM}}(0)} \tag{12}$$

where G_{XY} represents the projection of Π_{XY}^{I} along Π_{XY}^{M} and Π_{XY}^{Δ} is the remainder, the collision-induced component, which relaxes via mechanisms independent of collective reorientation. Within this projected representation

$$\Pi_{XY} = \Pi_{XY}^{\mathrm{R}} + \Pi_{XY}^{\Delta} \tag{13}$$

where

$$\Pi_{XY}^{\mathrm{R}} = (1 + G_{XY})\Pi_{XY}^{\mathrm{M}} \tag{14}$$

is the reorientational component. Hence, $(1 + G_{XY})$ represents the local field that modifies the portion of the PA that relaxes through collective reorientation.[28,29,33,36,37] Using eq 13, the PA-TCF can be separated in the following manner

$$\psi_{XY}(t) = \psi_{XY}^{\mathrm{RR}}(t) + \psi_{XY}^{\mathrm{R}\Delta}(t) + \psi_{XY}^{\Delta\Delta}(t) \tag{15}$$

https://doi.org/10.1021/acs.jpcb.0c11148
J. Phys. Chem. B 2021, 125, 3163−3177

Within the Born−Oppenheimer approximation, the third-order response function can be separated into its electronic and nuclear contributions[20]

$$R^{(3)} = R^{(3)\mathrm{el}} + R^{(3)\mathrm{nuc}} \tag{16}$$

The effectively instantaneous electronic portion can be expressed as a delta function in time

$$R^{(3)\mathrm{el}}_{\eta\gamma\beta\alpha}(t) = \sigma_{\eta\gamma\beta\alpha}\delta(t) \tag{17}$$

where η, γ, β, and α represent space indices in the laboratory frame. The electronic contribution therefore contains no information on molecular motions. The nuclear response function is proportional to the time-derivative of the (classical) correlation function of the components of the collective polarizability[1,17,20]

$$R^{(3)\mathrm{nuc}}_{\eta\gamma\beta\alpha}(t) = -\frac{\theta(t)}{k_\mathrm{B}T}\frac{\mathrm{d}}{\mathrm{d}t}\langle\Pi_{\eta\gamma}(t)\Pi_{\beta\alpha}(0)\rangle \tag{18}$$

where $\theta(t)$ is the Heaviside step function, k_B is the Boltzmann constant, and T is the temperature of the system. The experimental geometry used in OKE spectroscopy measures the anisotropic nuclear response function,[8,17] which is determined by the PA-TCF $\psi_{XY}(t)$

$$R^{(3)\mathrm{nuc}}_{XYXY}(t) = \frac{1}{2}[R^{(3)\mathrm{nuc}}_{XXXX}(t) - R^{(3)\mathrm{nuc}}_{XXYY}(t)]$$
$$\propto R(t) = -\frac{\theta(t)}{k_\mathrm{B}T}\frac{\mathrm{d}\psi_{XY}(t)}{\mathrm{d}t} \tag{19}$$

2.2. Computational and Simulation Details. Two different experimental molecular polarizability tensors have been reported for benzonitrile.[22,41] To determine which one is more accurate for our MD simulations, we first calculated it by ab initio quantum chemical methods with HF 6-311++G(d, p) using the Gaussian 03 package.[42] The calculated principal components of the molecular polarizability are α_{xx} = 11.6 Å^3, α_{yy} = 6.6 Å^3, and α_{zz} = 16.3 Å^3. These values are consistent with those previously reported (Bertucci et al.:[22] α_{xx} = 11.6 Å^3, α_{yy} = 8.2 Å^3, α_{zz} = 16.2 Å^3) and (Abdoul-Carime et al.:[41] α_{xx} = 11.2 Å^3, α_{yy} = 11.2 Å^3, α_{zz} = 15.0 Å^3), the main difference being a slightly larger change in α_{yy}. Clearly, the experimental results from Bertucci et al. are closer to the calculated values and were used in our MD simulations. The structure of benzonitrile is shown in Figure 1a. The molecular coordinate axes are defined with the y-axis normal to the ring plane and the z-axis parallel to the C−N bond direction. To improve the simulations of the dynamical and structural properties of benzonitrile, we modified the OPLS-AA force field[43] using the virtual atom method.[44] The virtual atom (dummy atom) method is a common method in molecular dynamics simulations and has been applied widely to macromolecules and small molecules, such as lipids, acetone, and water.[45−47] Benzonitrile has a 180° C_M−C≡N angle, which is straightforward to simulate with the virtual atom method. The atom masses of the C≡N bond are replaced with a new atom, M. The masses of the new atom, M, and the ring carbon, C_M, are redistributed while the corresponding C atom and N atom in the C≡N bond have no mass in the simulation. The new atom, M, is positioned at the center-of-mass of the C≡N bond. The redistribution rule ensures that the moment of inertia of the benzonitrile molecule is unchanged. In this modified force field, the M atom has no interactions with other atoms and functions solely as a mass center. The C and N atoms in the C≡N bond function as virtual atoms, which carry no mass but remain interaction centers. The modified OPLS-AA force field parameters for benzonitrile are given in Table S1 (Supporting Information). We also compared the dynamical and structural properties of benzonitrile calculated with the modified OPLS-AA force field, the standard OPLS-AA force field,[43] the general Amber force field,[48] and the Charmm general force field (see the Supporting Information).[49] These comparisons validate the accuracy of the modified OPLS-AA force field.

The model system consists of 1000 benzonitrile molecules in a cubic box of length 55.63 Å, with periodic boundary conditions. The MD program Gromacs 5.0 was used to calculate the dynamical and structural properties of benzonitrile in the bulk liquid at 300 K.[50,51] The cross interactions between unlike atomic sites on different molecules were computed by a sum of Coulomb and Lennard-Jones (6−12) terms with the Lorentz−Berthelot combination rules.[52] In all simulations, the bond lengths were constrained with the LINCS algorithm.[53] Note that the LINCS algorithm, like the SHAKE algorithm, constrains the bond lengths but the molecule remains flexible. The cut-off for Lennard-Jones interactions was taken as 12 Å. The long-range Coulomb interactions were handled by particle mesh Ewald (PME) with a cut-off of 12 Å and a grid spacing of 1.2 Å.[54] The Berendsen thermostat[52,55] was used in the *NPT* system to imitate the weak coupling between the system and a heat bath with a temperature coupling constant of 0.1 ps. The simulations were initially equilibrated in the isothermal−isobaric ensemble (*NPT*) at 1 atm for 5 ns. The systems were then further equilibrated in a constant volume−temperature (*NVT*) ensemble for 20 ns. Trajectories of an additional 40 ns following equilibration were sampled every 0.2 ps for analysis of the dynamics. In the *NVT* ensemble, a velocity rescaling thermostat[56] was used for the temperature coupling with a time coupling constant of 0.1 ps. The velocity rescaling thermostat can reproduce a more accurate kinetic ensemble than the Berendsen weak coupling method in an equilibrium system.

2.3. Reliability of the Modified Force Field. To validate the modified force field, we calculated a series of thermodynamic and dynamical properties of benzonitrile at different temperatures, that is, from 280 to 320 K. The simulations at different temperatures were conducted in an identical manner to the 300 K simulations. Trajectories of an additional 10 ns following equilibration were used for analysis. Figure 2 shows the temperature-dependent densities and compares them to the experimental values. These density values are very close to the experimental results.[57,58] The simulated densities also display a good linear relationship between the temperature and density. Simulating dynamical properties is vital because dynamics are directly related to whether the MD simulation can accurately reproduce the experimental dynamical observables discussed below. Hence, we compare the viscosities obtained using our modified force field to experimental values, as shown in Figure 3. The MD simulation results are in very good agreement with the experimental viscosities[57,59,60] over the entire temperature range. Our calculated results display a good Arrhenius temperature-dependent behavior. The local structure of liquid benzonitrile has been investigated with X-ray diffraction.[61] To compare the simulations to the X-ray diffraction results, we also calculated the liquid structure factor, as shown in Figure S5 of Supporting Information. Other

https://doi.org/10.1021/acs.jpcb.0c11148
J. Phys. Chem. B 2021, 125, 3163−3177

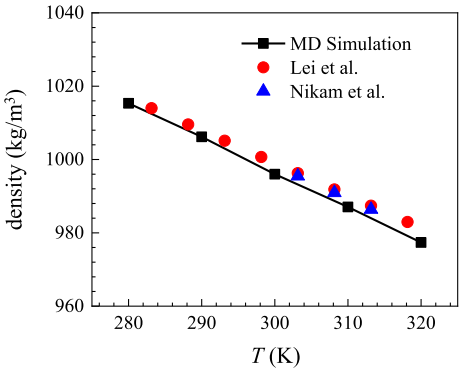

Figure 2. Comparison between the temperature-dependent density from the MD simulations using the modified force field and experimental measurements.

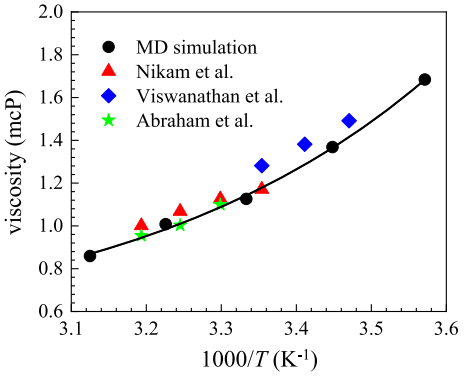

Figure 3. Comparison between the temperature-dependent viscosity from the MD simulations using the modified force field and the experimental measurements. The simulated viscosity values (black circles) were fit with the Arrhenius equation (solid curve).

properties including temperature-dependent self-diffusion coefficients and radial distribution functions (rdfs) obtained using the modified force field are also shown in the Supporting Information.

Table 1 displays select properties of benzonitrile calculated from the MD simulations with the modified force field and compares them to the experimental values and the classic force field simulation results at 300 K. The thermodynamic and dynamical properties obtained from the modified force field and classic force fields are very close to each other. The main exception is the generalized Amber force field, which produces larger errors in comparison to the experiments and the other force fields. Comparisons between the rdfs obtained with the modified OPLS-AA force field and other classic force fields can also be found in the Supporting Information. To summarize, the modified OPLS-AA force field for benzonitrile reproduces the measured thermodynamic, structural, and dynamical properties well and therefore can be used to simulate other structural and dynamical features of interest.

3. RESULTS AND DISCUSSION

3.1. Polarizability Anisotropy Time Correlation Function. In Figure 4, we present our main results, the

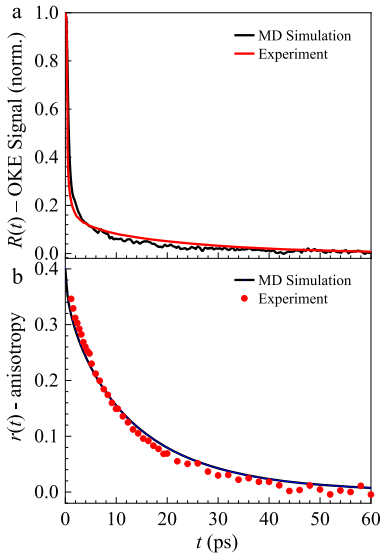

Figure 4. (a) Comparison of the simulated (black curve) and experimental (red curve) OKE signals of benzonitrile. (b) Simulated (black curve) and experimental (red points) anisotropy decays, $r(t) = 0.4C_2(t)$, for the C−N bond unit vector of benzonitrile.

simulated OKE signal, $R(t)$ (black curve, panel a), and the simulated anisotropy, $r(t)$ (black curve, panel b), which are compared to the experimental measurements for liquid benzonitrile[14] (red curve and red circles in panels a and b, respectively). As previously described, the PSPP experiment measures the anisotropy[3,4,14]

$$r(t) = 0.4C_2(t) = 0.4\langle P_2(\hat{\mathbf{u}}(0)\cdot\hat{\mathbf{u}}(t))\rangle \quad (20)$$

where $P_2(x) = (3x^2 - 1)/2$ is the second-order Legendre polynomial. The anisotropy is directly proportional to the orientational correlation function, $C_2(t)$, which is a measure of the correlation between the dipole moment unit vector residing on the same molecule at two times, making it an inherently single-molecule property. In contrast, the OKE signal depends on the collective polarizability tensor of the system and is therefore dependent on collective orientational variables. Consequently, whereas $\langle P_2(\hat{\mathbf{u}}_i(0)\cdot\hat{\mathbf{u}}_i(t))\rangle$ is the only contribution to the anisotropy, the OKE signal can, in general, have contributions from both $\langle P_2(\hat{\mathbf{u}}_i(0)\cdot\hat{\mathbf{u}}_i(t))\rangle$ and $\langle P_2(\hat{\mathbf{u}}_i(0)\cdot$

Table 1. Comparison of Experimental and Simulated Bulk Properties of Benzonitrile at 300 K Using Different Force Fields

	experiment	modified OPLS-AA force field	classic OPLS-AA force field[f]	Charmm force field	Amber force field
ρ^a(g/cm^3)	0.999	0.996	0.995	1.001	0.960
D^b(cm^2 s^{-1})	*8.3 × 10^{-6}	8.1 × 10^{-6}	8.0 × 10^{-6}	7.9 × 10^{-6}	1.2 × 10^{-5}
η^c(mPa s)	1.155	1.126	1.198	1.201	0.799
μ^d(D)	4.18	4.20	3.23	3.96	4.05
$C_p(l)^e$ (cal mol^{-1} K^{-1})	45.5	48.3	45.4	43.6	40.2

[a]Density.[38] [b]Translational diffusion coefficient, *approximate value (see the Supporting Information). [c]Viscosity.[57] [d]Permanent dipole moment.[38] [e]Molar heat capacity.[84] [f]See ref 43.

https://doi.org/10.1021/acs.jpcb.0c11148
J. Phys. Chem. B 2021, 125, 3163−3177

$\hat{\mathbf{u}}_j(t))\rangle$ terms. Additionally, interaction- or collision-induced effects in liquids can constitute a significant portion of the spectral density,[3,33] thus these many-body effects must be included to accurately describe the effective polarizability tensor. As seen in Figure 4, the simulations using the modified OPLS-AA force field (black curves) reproduce both observables quantitatively. The two types of data reflect results of distinct experimental methods and measure different dynamic properties of the system. Considering the fundamentally different nature of the OKE signal and anisotropy, the former collective-relaxation arising from a non-resonant Raman interaction[3,8] and the latter single-molecule relaxation arising from a resonant dipole interaction,[1−3] the ability of the polarizability model and modified force field to reproduce both observables is a stringent confirmation of the calculation methods. The underlying structures and dynamics influencing the time scales of relaxations will be analyzed in detail below.

In Figure 5, we analyze the time integral of $R(t)$, or the PA-TCF, $\psi(t)$, of benzonitrile (solid black curve). The PA

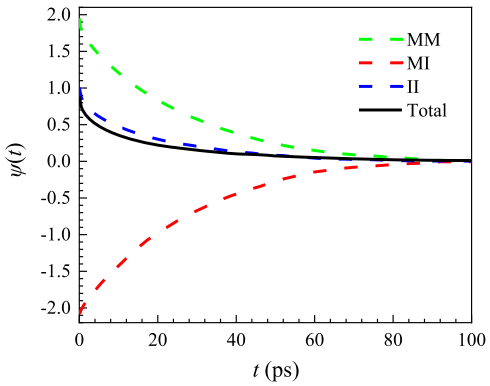

Figure 5. PA-TCF (solid black curve) of benzonitrile at 300 K. The contributions of the molecular (dashed lime-green curve) and interaction-induced (dashed blue curve) autocorrelations, and their cross-correlation (dashed red curve) are displayed for comparison to the PA-TCF.

relaxation of benzonitrile decays over roughly 100 ps. This decay is very slow in comparison to that of acetonitrile, which decays completely within 5 ps,[62,63] although both molecules contain a single, polar CN bond. The relaxation dynamics are also ∼10 times slower than the similar sized molecule benzene.[64−66] Therefore, it appears that the combination of the larger size of benzonitrile and the presence of the CN moiety greatly slows the dynamics.

To understand the origin of the slow relaxation mechanism, the contributions from the auto- and cross-correlations of the molecular- and interaction-induced components of the collective polarizability are shown in addition to the total PA-TCF in Figure 5. Recall from eq 9 that the total PA-TCF can be expressed as the sum of these three contributions: $\psi^{MM}(t)$, $\psi^{MI}(t)$, and $\psi^{II}(t)$. First, notice that the $\psi^{MI}(t)$ contribution (dashed red curve) is negative. This decay follows a similar in magnitude, but opposite signed, trend to the $\psi^{MM}(t)$ contribution (dashed lime-green curve). The net result is that the $\psi^{MI}(t)$ and $\psi^{MM}(t)$ TCFs nearly cancel each other, leaving $\psi^{II}(t)$ (dashed blue curve) as the main influence on the total decay. This is evidenced by the close resemblance between $\psi^{II}(t)$ and $\psi(t)$ in terms of their magnitude and time-dependence. Additionally, Figure 5 demonstrates that all three TCFs, $\psi^{MM}(t)$, $\psi^{MI}(t)$, and $\psi^{II}(t)$, contribute significantly to $\psi(t)$ over the complete time range of the relaxation. If $\psi^{MM}(t)$ was the only contributor to the decay for longer times, we could conclude that the longer relaxation originates from collective reorientation. However, all three contribute significantly, meaning that the influence of $\mathbf{\Pi}^{I}$, which is modulated by both translations and rotations, is significant at all times. Therefore, as has been found for many smaller molecules,[28,29,34−37] this natural manner of decomposing $\psi(t)$ does not clarify whether a clear separation in time scales exists between the collision-induced and collective reorientation relaxation mechanisms of benzonitrile.

To gauge how collective reorientation governs the relaxation process, we recast $\psi(t)$ in a projected representation[33] in which the portion of $\mathbf{\Pi}^{I}$ that has the same time-dependence as $\mathbf{\Pi}^{M}$ is separated out (eqs 11−15). The PA-TCF is now expressed as the sum of the three components: $\psi^{RR}(t)$, $\psi^{R\Delta}(t)$, and $\psi^{\Delta\Delta}(t)$. The results of this projected representation are shown in Figure 6. Overall, the reorientational component, $\psi^{RR}(t)$

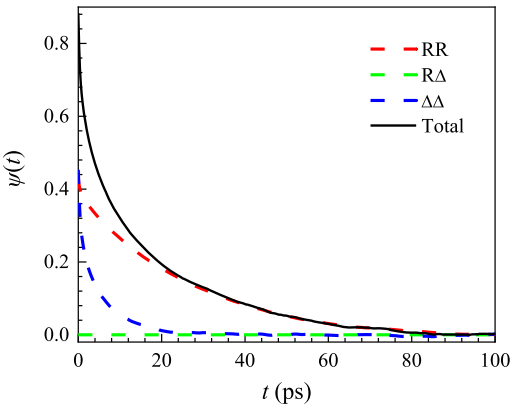

Figure 6. Components of the PA-TCF in the projected representation. The contributions of the reorientational (dashed red curve) and collision-induced (dashed blue curve) autocorrelations and their cross-correlation (dashed lime-green curve) are displayed for comparison to the PA-TCF (solid black curve).

(dashed red curve), is the largest contributor to $\psi(t)$ (solid black curve). However, $\psi^{RR}(t)$ is by no means dominant, especially in the short-time relaxation. The collision-induced contribution, $\psi^{\Delta\Delta}(t)$ (dashed blue curve), is significant in the early time range of 0−20 ps and causes $\psi(t)$ to decay much faster than the reorientational component, $\psi^{RR}(t)$. However, following 20 ps, the reorientational component dominates $\psi(t)$, and the two decays are essentially identical beyond that point. Notably, the cross-term, $\psi^{R\Delta}(t)$ (dashed lime-green curve), makes a negligible contribution. Therefore, this alternate representation of the collective polarizability and the PA-TCF reveals that reorientational and collision-induced dynamics both contribute significantly at early times, but beyond 20 ps, collective reorientation dominates the PA-TCF. Comparing Figures 5 and 6, it is seen that $\psi^{RR}(0)$ is about half of the value of the PA-TCF, $\psi(0)$, and one-fourth the value of $\psi^{MM}(0)$. These relationships are reflected in the projection factor $G = -0.53$ (eq 12) for benzonitrile. From eqs 8 and 14, $\psi^{RR} = (1 + G)^2\psi^{MM}$, which means that, in the case of benzonitrile, the local field factor $(1 + G)^2$ greatly decreases the magnitude of the collective reorientation contribution to $\psi(t)$.

To assess the time scale of collective reorientation, we return to Figure 4a which compares the simulated OKE signal, $R(t)$,

https://doi.org/10.1021/acs.jpcb.0c11148
J. Phys. Chem. B 2021, 125, 3163−3177

to the recently reported measurement.[14] The simulated signal agrees well with the experimental signal over the entire relaxation process. Note, however, that numerical differentiation of the PA-TCF to obtain $R(t)$ amplifies the noise present in $\psi(t)$. This noise is particularly obvious in the long-time relaxation, especially when plotted on a semi-log plot (see Figure S9). Some authors previously made use of a sum of Gaussian and exponential functions to fit the simulated OKE response function and then compared the fit curve with experimental results.[29] This procedure agrees fairly well with the experiments but may introduce some error into the determination of the long-time scale relaxation. Although noise is evident in the simulation at long time, our simulated data reproduce the experiment well without fitting to a complicated functional form.

Many experimental studies have focused on fitting the decay of $R(t)$ that occurs beyond ~2 ps, sometimes with a multi-exponential function.[7,67] Our previous experimental study of benzonitrile found that a single-exponential fit was sufficient to model the long-time OKE decay.[14] Hence, we also use a single exponential to fit the simulated OKE signal from 20 to 80 ps (see Figure S10). As the main focus of this study is to understand the reorientation dynamics of benzonitrile, we begin at 20 ps because the collision-induced contribution dies out by that time and collective reorientation dominates the PA-TCF, $\psi(t)$ (Figure 6). This simple fitting procedure yields a time constant for collective reorientation, $\tau_c = 28.8 \pm 1.1$ ps, that is slightly larger than the OKE experimental value of 20.4 ± 1 ps.[14,27] This difference may be ascribed, in part, to the greater noise in the long-time relaxation of the simulated signal, $R(t)$. However, considering that the simulation correctly captures both measurements in Figure 4a,b, this difference is not significant.

3.2. Orientational Pair Correlations. The influence of static and dynamic orientational pair correlations (OPCs) on the PA-TCF can be evaluated by decomposing $\psi_{XY}^{MM}(t)$ into contributions from single molecules and pairs

$$\psi_{XY}^{MM}(t) = \frac{1}{\Gamma^2}\sum_{i=1}^{N}\sum_{j=1}^{N}\langle \alpha_{i,XY}(0)\alpha_{j,XY}(t)\rangle = \psi_{XY}^{MM,s}(t) + \psi_{XY}^{MM,p}(t) \quad (21)$$

where the single-molecule (or self) contribution is

$$\psi_{XY}^{MM,s}(t) = \frac{1}{\Gamma^2}\sum_{i=1}^{N}\langle \alpha_{i,XY}(0)\alpha_{i,XY}(t)\rangle \quad (22)$$

and the pair (or distinct) contribution is

$$\psi_{XY}^{MM,p} = \frac{1}{\Gamma^2}\sum_{i=1}^{N}\sum_{j\neq i}\langle \alpha_{i,XY}(0)\alpha_{j,XY}(t)\rangle \quad (23)$$

Figure 7 compares $\psi_{XY}^{MM}(t)$ (black curve) with its two contributions, $\psi_{XY}^{MM,s}(t)$ (red curve) and $\psi_{XY}^{MM,p}$ (blue curve). The single-molecule portion, $\psi_{XY}^{MM,s}(t)$, exhibits a faster decay than either the full molecular TCF, $\psi_{XY}^{MM}(t)$, or the pair-contribution, $\psi_{XY}^{MM,p}$, which is responsible for the decay at long time. The $\psi_{XY}^{MM,p}$ contribution is larger than that of $\psi_{XY}^{MM,s}(t)$ after very early times, a result that is reminiscent of what was found for 1,3,5-trifluorobenzene in a previous MD study.[36] The magnitude of the pair-contribution displayed in Figure 7 immediately indicates the presence of OPCs in benzonitrile. The static second rank OPC factor, which quantifies

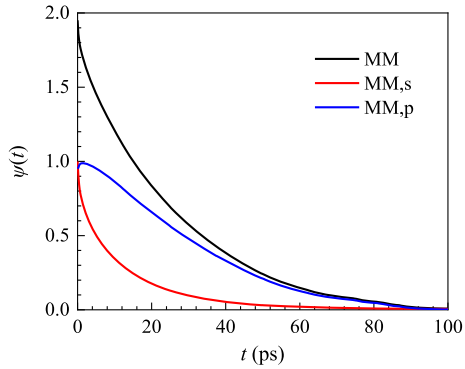

Figure 7. Comparison of the molecular polarizability anisotropy autocorrelation, $\psi^{MM}(t)$, (black curve) and its single-molecule, $\psi^{MM,s}(t)$, (red curve) and pair, $\psi^{MM,p}(t)$, (blue curve) contributions.

correlations between molecular anisotropic polarizability components, is given by the initial value of $\psi_{XY}^{MM}(t)$[40,68−70]

$$g_2 = \psi_{XY}^{MM}(0) = \frac{\langle(\Pi_{XY}^{M})^2\rangle}{\Gamma^2} = \psi_{XY}^{MM,s}(0) + \psi_{XY}^{MM,p}(0) \quad (24)$$

Note that $\psi_{XY}^{MM,s}(0) = 1$ by definition, and therefore, $g_2 = 1$ would indicate the absence of OPCs. A nonzero $\psi_{XY}^{MM,p}(0)$ modifies the reference unity value. The magnitude and sign of the deviation from unity reflect the strength and nature of the orientational structure in the liquid.

To see how g_2 is related to the liquid structure, it is useful to consider the simpler case of an axially symmetric molecule ($\alpha_{xx} = \alpha_{yy} = \alpha_\perp$ and $\alpha_{zz} = \alpha_\parallel$), such as acetonitrile.[29,71] The polarizability tensor of an axially symmetric molecule can be expressed as[40]

$$\alpha_{\alpha\beta} = \alpha_0\delta_{\alpha\beta} + \gamma\left[u_\alpha u_\beta - \frac{1}{3}\delta_{\alpha\beta}\right] = \alpha_0\delta_{\alpha\beta} + \gamma_{\alpha\beta} \quad (25)$$

where $\delta_{\alpha\beta}$ is the Kronecker delta, $\alpha_0 = (2\alpha_\perp + \alpha_\parallel)/3$ is the isotropic part of the polarizability tensor, $\gamma = \alpha_\parallel - \alpha_\perp$ is the anisotropic part, and u_α is the αth component of $\hat{\mathbf{u}}$, a unit vector along the molecular symmetry axis (parallel to the CN bond for acetonitrile). Note that the $\alpha_0\delta_{\alpha\beta}$ portion of the tensor $\boldsymbol{\alpha}$ is rotationally invariant, while the anisotropic part, $\gamma_{\alpha\beta}$, changes as the molecule rotates through its dependence on $\hat{\mathbf{u}}$. From eq 25

$$\langle\gamma_{i,\alpha\beta}(0)\gamma_{j,\alpha\beta}(t)\rangle = \gamma^2\left\langle\left[u_{i,\alpha}(0)u_{i,\beta}(0) - \frac{1}{3}\delta_{\alpha\beta}\right]\left[u_{j,\alpha}(t)u_{j,\beta}(t) - \frac{1}{3}\delta_{\alpha\beta}\right]\right\rangle = \frac{2}{3}\gamma^2\langle P_2[\hat{\mathbf{u}}_i(0)\cdot\hat{\mathbf{u}}_j(t)]\rangle \quad (26)$$

where $P_2(x) = (3x^2 - 1)/2$ is the second-order Legendre polynomial. It can be further shown[40] that

https://doi.org/10.1021/acs.jpcb.0c11148
J. Phys. Chem. B 2021, 125, 3163−3177

$$\langle \alpha_{i,XY}(0)\alpha_{j,XY}(t)\rangle = \frac{\langle \gamma_{i,\alpha\beta}(0)\gamma_{j,\alpha\beta}(t)\rangle}{10} = \frac{\gamma^2}{15}\langle P_2[\hat{\mathbf{u}}_i(0)\cdot\hat{\mathbf{u}}_j(t)]\rangle \quad (27)$$

Therefore, g_2 (eq 24) can be rewritten as

$$g_2 = 1 + \frac{1}{N}\sum_{i=1}^{N}\sum_{j\neq i}\langle P_2[\hat{\mathbf{u}}_i(0)\cdot\hat{\mathbf{u}}_j(0)]\rangle \quad (28)$$

The quantity $\hat{\mathbf{u}}_i(0)\cdot\hat{\mathbf{u}}_j(0) = \cos\theta_{ij}$, where θ_{ij} is the angle between the symmetry axes of the ith and jth molecules at time zero. A plot of $P_2(\cos\theta)$ is shown in Figure S11. It has two roots, one at the magic angle ~54.7° and another at its supplement ~125.3°. For angles between these two values, the molecules are oriented in a more perpendicular arrangement, $P_2(\cos\theta)$ is negative on average, and g_2 is less than 1. Positive deviations, in which g_2 is greater than 1, are observed between the ranges 0 to 54.7 and 125.3 to 180°, which reflect parallel and antiparallel arrangements, respectively.

In contrast to acetonitrile, α_{xx} and α_{yy} differ to some extent for benzonitrile, which classifies it as an asymmetric molecule.[39,40] In this case, g_2 is not simply related to the angle between the CN bond unit vectors but rather represents a sort of weighted average of static OPC factors for all three principal axes.[72] Equation 28 becomes more valid as α_{xx} and α_{yy} approach the same value. From our simulated TCF, $\psi^{MM}(0)$, we find $g_2 = 1.95$, which is much larger than 1. This value implies that a local parallel or antiparallel ordering structure may be present in liquid benzonitrile. The presence of these local structures will be explored in the following section.

In the rotational diffusion limit, the parameter g_2 can also be related to the collective and single-molecule orientational relaxation times, τ_c and τ_s, respectively, through the expression[40,70,72]

$$\tau_c = (g_2/j_2)\tau_s \quad (29)$$

where j_2 is the dynamic OPC factor. The above expression was derived for the case of a symmetric top and therefore can only expected to be approximately true in the most general case.[72] Experimentally, τ_c was determined by fitting the long-time optical-heterodyne detected OKE signal to a single-exponential decay.[14] The single-molecule correlation time, τ_s, was obtained by performing IR PSPP experiments on the naturally abundant ^{13}CN stretch mode. The measured anisotropy decay, which is shown in Figure 4b (red points), was found to be biexponential.[14] It was previously argued that the first-time constant results from restricted angular diffusion, or wobbling-in-a-cone dynamics, and the second-time constant arises from free rotational diffusion.[14] Thus, τ_s was obtained from the long-time decay in the anisotropy, $r(t)$.

Both τ_c and τ_s were obtained from the MD simulations in an analogous manner to the experiments. The determination of τ_c was discussed in Section 3.1. The single-molecule time, τ_s, was obtained from the simulated anisotropy for the unit vector $\hat{\mathbf{u}}$ along the CN bond of benzonitrile (Figure 4b, black curve). As can be seen from the figure, the simulated reorientation dynamics not only agree well with the experimental data but also reveal femtosecond inertial dynamics which were too fast to detect in the experiments. The simulated $r(t)$ function is likewise fit well with a biexponential decay. However, for reasons discussed above, τ_s was determined by fitting the simulated $C_2(t)$ out to long time starting from 20 ps. The value obtained from this fitting procedure was $\tau_s = 17.2 \pm 0.1$ ps (see Figure S12). As was found for τ_c in Section 3.1, this value for τ_s is very close, only slightly larger than the experimental value of 13.1 ps.[14] Note that τ_s could alternatively be obtained from fitting $\psi_{XY}^{MM,s}(t)$, whose relaxation is dictated by single-molecule rotational motion. In Figure S13, $\psi_{XY}^{MM,s}(t)$ and $C_2(t)$ for the z axis are displayed on the same plot to illustrate their effectively identical time-dependence. From eqs 22 and 27, one would expect these TCFs to be equivalent in the limit of a symmetric molecule.

Substituting the simulated values of τ_c and τ_s into eq 29 provides the ratio $g_2/j_2 = 1.67 \pm 0.07$. This value is close to the previous experimental value of 1.56.[14] The result is also in agreement with the result of Alms and Patterson, who obtained a value of 1.58 from analysis of the depolarized Rayleigh spectrum of benzonitrile.[23] The dynamic OPC parameter j_2 is generally assumed or observed to be very close to 1 in the majority of experimental investigations,[22,23,27,40,71,73] implying an absence of dynamic OPCs. By substituting $g_2 = 1.95$, found above, into eq 29, the value $j_2 = 1.17$ is obtained. It should be noted that this manner of estimating j_2 depends on how well τ_c and τ_s can be determined and the extent to which eq 29 is a good approximation for benzonitrile. The results of Figure S13 indicate that this is a reasonable approach. The value of j_2 obtained suggests that a small extent of dynamical orientational correlation exists. In our view, a more complete analysis and comparison of j_2 in liquids with different structural characteristics and intermolecular interactions are still needed.

3.3. Local Structure. The result $g_2 = 1.95$ from Section 3.2 implies that an ordered local structure is present in benzonitrile. Previous simulations demonstrated that similar sized aromatic molecules exhibited local structures with varying types and degrees of ordering.[36] For example, 1,3,5-trifluorobenzene exhibits a prominent stacked dimer structure that makes the symmetry axes (normal to the ring) parallel. At close distances, hexafluorobenzene displays some stacking but has perpendicular configurations at larger separations. Benzene displays a nearly isotropic local order.

It is experimentally challenging to observe the local nanoscale structures in a liquid, although a previous X-ray diffraction study has presented some evidence of antiparallel stacking in benzonitrile.[61] This information can be directly obtained from an MD simulation study by analyzing the radial−angular pair correlation function $g(r,\theta)$, defined as

$$g(r,\theta) = \frac{1}{N\rho(r,\theta)}\left\langle \sum_{i\neq j}^{N}\delta(r - r_{ij})\delta(\theta - \theta_{ij})\right\rangle \quad (30)$$

where $\rho(r,\theta)$ represents the number of molecules, defined as $(N/V)2\pi r^2\Delta r\Delta\theta\sin\theta$, Δr and $\Delta\theta$ are the radial and angular resolutions, and r_{ij} and θ_{ij} are the intermolecular distance between the center positions of the C−N bonds and the angle between the C−N bond directions of molecules i and j, respectively. The angular and radial resolutions were taken to be $\Delta\theta = 1°$ and $\Delta r = 0.02$ nm, respectively.

Figure 8 shows the radial−angular pair correlation function for benzonitrile at 300 K. An intense peak is located at $\theta = 175°$ centered around $r = 0.34$ nm. This is a strong signature of an antiparallel arrangement of neighboring benzonitrile molecules. The function $g(r,\theta)$ swiftly declines from its global maximum, $g(0.34\text{ nm}, 175°) = 9.24$, moving toward smaller

https://doi.org/10.1021/acs.jpcb.0c11148
J. Phys. Chem. B 2021, 125, 3163−3177

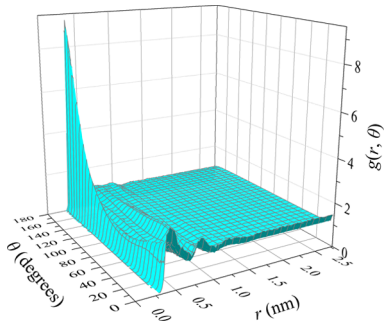

Figure 8. Radial−angular pair correlation function for benzonitrile at 300 K. The pair distance, r, and the angle, θ, are defined as the intermolecular distance between the center positions of the C−N bonds and the angle between the C−N bond directions of molecules i and j, respectively.

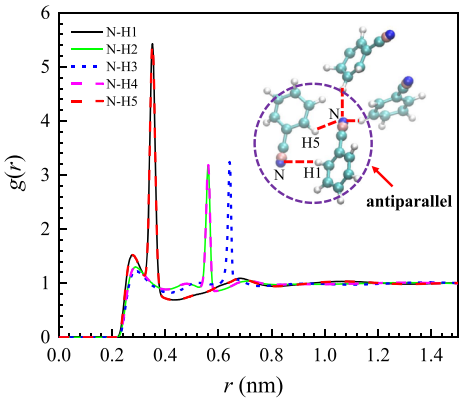

Figure 9. Rdfs between the N atom and H atom sites on different benzonitrile molecules. The peaks in the N−H rdfs represent the intensity of different Coulombic interaction motifs in the bulk liquid. The inset displays a representative structure observed in the MD simulation of the benzonitrile liquid featuring antiparallel nearest neighbors.

angles. A smaller local maximum can be seen near g(0.44 nm, 1°), corresponding to benzonitrile molecules arranged in a parallel orientation. Another local maximum with a broad distribution at small angles is seen near 0.84 nm, although this broad peak is lower than the former two peaks. These additional peaks indicate that parallel structures also exist in liquid benzonitrile at greater pair distances. However, the dominant configuration is the antiparallel one. Both parallel and antiparallel arrangements cause the static OPC parameter, g_2, to be much greater than 1. These MD simulation results support previous conclusions that a pronounced antiparallel structure exists in benzonitrile.[14,61,74]

The forces driving the formation of OPCs have not been fully elucidated. Moreover, the relevant factors appear to depend on the system under study. In certain systems, molecular shape and packing are important driving forces. For example, calculation of the liquid structure of acetonitrile with a reference interaction site model revealed strong OPCs between neighboring molecules.[75] Another study investigated several mono-substituted derivatives of benzene (including benzonitrile) with DRS, the frequency-domain analogue of OKE spectroscopy, and found that the magnitude of the OPCs was correlated with the square of the molecular dipole moment.[22] It has been suggested that an antiparallel arrangement of the symmetry axes of neighboring molecules aligns their electron-rich and electron-deficient regions in a favorable manner.[22]

We further investigated the role of intermolecular interactions in the formation of antiparallel configurations in benzonitrile. In particular, the partial negative charge on the nitrogen atom of the polar C−N bond can have significant Coulombic interactions with the small partial positive charges of hydrogen atoms on nearby benzonitrile molecules. The site−site rdfs between the nitrogen atom and different hydrogen atom sites are displayed in Figure 9. Large, overlapped peaks corresponding to N−H1/N−H5 interactions are observed at 0.35 nm. The H1 and H5 sites are functionally equivalent and the most electropositive, owing to their ortho-substitution relative to the C−N bond. Smaller peaks centered at 0.56 and 0.64 nm, corresponding to N−H2/N−H4 and N−H3 interactions, respectively, are also observed. These rdfs demonstrate that the nitrogen atom can form multiple significant Coulombic interactions with different hydrogen sites on adjacent molecules. However, the most important Coulombic interaction is the N−H1/N−H5 interaction. These Coulombic interactions are maximized when two-neighboring molecules orient their symmetry axes in an antiparallel configuration. The average N−H1/N−H5 distance in our simulation system is about 0.327 nm. Considering the charges of the N atom and the H1/H5 atoms, we can calculate the interaction energy of this strong C−N···H1/H5 interaction using Coulomb's law. The calculated value is about 24.4 kJ/mol, which is very close to the typical hydrogen bond interaction energy. Therefore, the N−H1/N−H5 Coulombic interaction is an important driving force for the large peak in the radial−angular pair correlation function at large angles corresponding to the antiparallel arrangement. A representative snapshot of a structure present in bulk benzonitrile with multiple significant Coulombic interactions is shown in the inset in Figure 9.

3.4. Orientational Dynamics and Rotational Diffusion. The PSPP experiment is only sensitive to the dynamics of the unit vector $\hat{\mathbf{u}}$, which coincides with the z direction in the molecular frame of benzonitrile (Figure 1a). Thus, previous experiments could not observe the dynamics in the x and y directions. With the limited information obtained from observing only the dynamics of the CN bond, it was determined that the rotational diffusion coefficients in the x and y directions were approximately equal.[14]

From the MD simulation, we can calculate the orientational dynamics in all three directions. In Figure 10, $C_2(t)$ is plotted for unit vectors along the x, y, and z directions. Clearly, $C_2(t)$ differs between the three directions, indicating that the rotational dynamics of benzonitrile are spatially anisotropic. However, the dynamics in the x and y directions are similar to each other and differ more substantially from the slower dynamics observed for the z direction. These $C_2(t)$ decays can be fit to a sum of three exponentials. Table 2 displays the fit parameters for the three principal axis directions. The first-time constant, t_1, is on the order of 500 fs for all directions. This time scale lies within the inertial regime of orientational dynamics, which occurs on a similar time scale to that of the translational velocity autocorrelation function decay (see Figure S14), in which a small degree of angular sampling occurs via rapid collisions with adjacent solvent molecules. This time scale was not resolved in previous experiments. The simulations slightly overestimate the FD correlation times. Therefore, it is also expected that the rapid ballistic dynamics

https://doi.org/10.1021/acs.jpcb.0c11148
J. Phys. Chem. B 2021, 125, 3163−3177

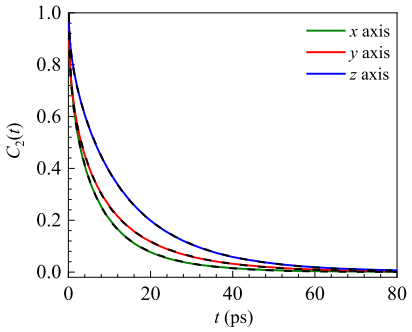

Figure 10. Second-order Legendre polynomial orientational correlation functions, $C_2(t)$ (solid curves), for unit vectors along the x (green), y (red), and z (blue) principal axes of benzonitrile (see Figure 1). The black dashed curves, which lie directly on top of the simulated curves, are multi-exponential fits.

from the simulations are slower than that would be observed in an experiment. The second-time constant, t_2, ranges from ∼4 to 6 ps depending upon the direction observed. It is slowest for the z direction, which was observed experimentally to be 3.8 ± 1.0 ps.[14] This component of the decay arises from restricted angular diffusion, which was previously modeled with a wobbling-in-a-cone correlation function. As discussed in Section 3.3, the local molecular structure indicates that the electronegative N atom of the CN group has multiple significant Coulombic interactions with the hydrogen atoms on nearby benzonitrile molecules. The significant Coulombic attractive forces constitute directional interactions that impose restrictions on reorientation, and such interactions must be broken to permit FD of the molecule. The third relaxation time, t_3, is equivalent to τ_s, the single-molecule FD correlation time. For the z direction, it is 17.0 ps, which agrees with the value of 17.2 ps obtained from a single-exponential fit to the long-time relaxation in Section 3.2.

The orientation of a vector changes when rotations occur around the two axes normal to the vector. For example, the $C_2(t)$ dynamics for a vector along the z axis are determined by rotational diffusion occurring around the x and y directions. Thus, the slow reorientation dynamics observed for the vector $\hat{\mathbf{u}}$ along z (Figure 4b) implies slow rotational diffusion about the x and y axes. From inspection of the $C_2(t)$ decays in Figure 10, the free rotational diffusion coefficients can be ordered from largest to smallest: $D_{zz} > D_{yy} > D_{xx}$. To further validate and quantify this ordering, we calculated the rotational diffusion coefficients in all three directions. This was accomplished by calculating the RMSD, $\langle \phi^2(t) \rangle = 4D_r t$. Our calculation was based on the method used by Mazza et al.,[76] extended to the three principal axes in the molecular frame of benzonitrile. This method avoids the quantity boundary issue that is encountered when the vector under consideration is bounded to the unit sphere (details in the Supporting Information). Figure 11 displays the RMSDs for unit vectors along the three principal axes. Clear linear trends are found in

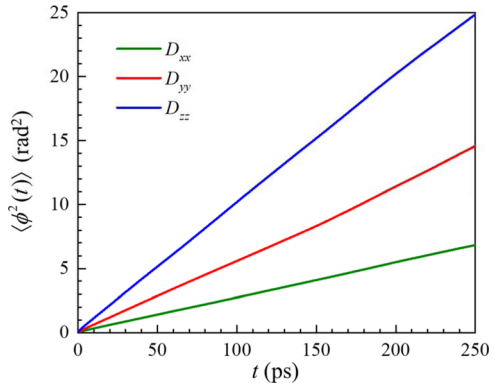

Figure 11. RMSD as a function of time for the three principal axes of benzonitrile. The relation $\langle \phi^2(t) \rangle = 4D_r t$ was used to calculate the rotational diffusion coefficients from the linear regimes of the curves.

all directions after very short times. The calculated rotational diffusion coefficients are $D_{xx} = 6.8 \times 10^{-3}$ ps^{-1}, $D_{yy} = 1.46 \times 10^{-2}$ ps^{-1}, and $D_{zz} = 2.48 \times 10^{-2}$ ps^{-1}, respectively. These values follow the expected trend $D_{zz} > D_{yy} > D_{xx}$ deduced from the $C_2(t)$ correlation functions in Figure 10. In our previous experimental study, in which only the $C_2(t)$ decay for the z (CN bond) direction could be measured, we assumed that $D_{xx} \simeq D_{yy}$.[14] Here, we elucidated the complex rotational diffusion in liquid benzonitrile that results from the asymmetric shape of the molecule. The experimental value, referred to as $D_\perp$, was found to be 1.27×10^{-2} ps^{-1},[14] which falls between the values of D_{xx} and D_{yy} calculated here.

3.5. FD of an Asymmetric Rotor and Wobbling-in-a-Cone. The simulated $C_2(t)$ correlation functions (Figure 10) can be modeled in more detail now that the rotational diffusion coefficients have been independently determined. The rotational diffusion of a completely asymmetric rotor has been treated previously.[18,77−81] This theory relates the amplitudes and time scales of $C_2(t)$ to the principal components of the rotational diffusion tensor. For unit vectors fixed along the x, y, and z principal axes of benzonitrile, the following (FD) expressions are obtained[14,81]

Table 2. Multi-Exponential Fit Parameters for $C_2(t)$[a]

axis	A_1	t_1 (ps)	A_2	t_2 (ps)	A_3	t_3 (ps)
x	0.24 ± 0.02	0.47 ± 0.07	0.35 ± 0.03	3.9 ± 0.5	0.40 ± 0.04	12.0 ± 0.6
y	0.25 ± 0.02	0.45 ± 0.06	0.34 ± 0.02	4.39 ± 0.04	0.41 ± 0.03	15.6 ± 0.5
z	0.15 ± 0.01	0.55 ± 0.01	0.24 ± 0.03	6 ± 1	0.62 ± 0.04	17.0 ± 0.5
z (expt.)			0.19 ± 0.05	3.8 ± 1	0.79 ± 0.05	12.8 ± 0.5

[a]The experimental data are reproduced with permission from Yamada et al., J. Phys. Chem. B **122**, 12147-12153 (2018). Copyright 2018 American Chemical Society.

https://doi.org/10.1021/acs.jpcb.0c11148
J. Phys. Chem. B 2021, 125, 3163−3177

$$C^{x}_{2,\mathrm{FD}}(t) = \frac{3}{12N^2}[(a^2 - 2\sqrt{3}ab + 3b^2)\mathrm{e}^{-(6D+2\Delta)t} + (b^2 + 2\sqrt{3}ab + 3a^2)\mathrm{e}^{-(6D-2\Delta)t}]$$

$$C^{y}_{2,\mathrm{FD}}(t) = \frac{3}{12N^2}[(a^2 + 2\sqrt{3}ab + 3b^2)\mathrm{e}^{-(6D+2\Delta)t} + (b^2 - 2\sqrt{3}ab + 3a^2)\mathrm{e}^{-(6D-2\Delta)t}]$$

$$C^{x}_{2,\mathrm{FD}}(t) = \frac{1}{N^2}[a^2\,\mathrm{e}^{-(6D+2\Delta)t} + b^2\,\mathrm{e}^{-(6D-2\Delta)t}] \quad (31)$$

where the parameters in eq 31 are completely determined by the three diffusion coefficients D_{xx}, D_{yy}, and D_{zz}:

$$a = \sqrt{3}\,(D_{xx} - D_{yy}),$$

$$b = 2D_{zz} - D_{xx} - D_{yy} + 2\Delta, \qquad N = 2(\Delta b)^{1/2}$$

$$\Delta = [(D_{xx} - D_{yy})^2 + (D_{zz} - D_{xx})(D_{zz} - D_{yy})]^{1/2}$$

$$D = \frac{1}{3}(D_{xx} + D_{yy} + D_{zz}) \quad (32)$$

From eq 31, it is clear that, regardless of which direction is probed, $C_2(t)$ is a biexponential function with two time constants given by $\tau_1 = (6D + 2\Delta)^{-1}$ and $\tau_2 = (6D - 2\Delta)^{-1}$. Substituting in the values of the diffusion coefficients obtained in Section 3.4, we obtain $\tau_1 = 8.1$ ps and $\tau_2 = 16.4$ ps. The FD limit correlation functions of eq 31 are plotted alongside the simulated $C_2(t)$, as shown in Figure 12a. Although the qualitative trend with respect to direction is correct, the theoretical and simulated correlation functions do not match. As discussed previously, the rotational dynamics at early times involve a non-diffusive inertial regime as well as restricted rotational diffusion, previously characterized with the wobbling-in-a-cone model.[14] These processes also contribute to the decay of $C_2(t)$ at early times, leading to apparent disagreement between the theory and simulation.

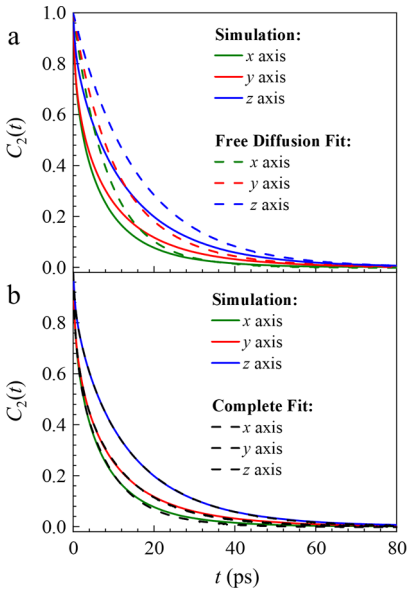

Figure 12. (a) Predicted fits from the FD theory for an asymmetric rotor, applied to benzonitrile (dashed curves), are compared to the simulated $C_2(t)$ (solid curves) for the three principal axis directions, x (green), y (red), and z (blue). (b) Same comparison in (a) with the inclusion of ballistic motion and wobbling-in-a-cone dynamics to the fit (black dashed curves). The agreement is substantially improved.

A single wobbling-in-a-cone process can be described by an approximate correlation function of the form, $C_2(t) = Q^2 + (1 - Q^2)\exp[-t/\tau_c]$.[30,31,82] The long-time offset of the correlation function is given by the generalized order parameter $Q^2 = [\{\cos\theta_c(1 + \cos\theta_c)\}/2]^2$, where θ_c is the half-angle of the cone in which the diffusing transition dipole vector is confined. Although the inertial reorientation is not diffusive, and is strictly Gaussian at early time,[83] we approximate it by a separate wobbling-in-a-cone process (i.e., a single exponential with an offset). Treating these as independent processes, the complete expression for $C_2(t)$ is given by

$$C^{\alpha}_{2}(t) = (T^2 + (1 - T^2)\exp[-t/\tau_{\mathrm{in}}])(S^2 + (1 - S^2)\exp[-t/\tau_c])C^{\alpha}_{2,\mathrm{FD}}(t) \quad (33)$$

where T, τ_{in}, S, and τ_c are the order parameter and correlation time for the inertial cone and diffusive cone, respectively. In eq 33, the $C^{\alpha}_{2,\mathrm{FD}}(t)$ expressions for a unit vector fixed along the α principal axis in the molecular frame are given by eq 31. We note that in our previous experimental study of the reorientation of ^{13}CN benzonitrile, the inertial process, which was too short to be observed, was treated as instantaneous.[14] The inertial cone correlation function in eq 33 was then simplified to T^2. The approximation $D_{xx} = D_{yy} = D_{\perp}$ was also made, which led to the simplified expression $C^{z}_{2,\mathrm{FD}}(t) = \exp[-t/\tau_{\perp}]$, where $\tau_{\perp} = 1/6D_{\perp}$. Therefore, the resulting biexponential function

$$r(t) = 0.4C^{z}_{2}(t) = 0.4T^2(S^2 + (1 - S^2)\exp[-t/\tau_c])\exp[-t/\tau_{\perp}] \quad (34)$$

was used previously to analyze the experimental anisotropy data.

The fits of eq 33 to the simulated $C_2(t)$, using the appropriate correlation functions from eq 31, are shown for all three directions in Figure 12b. In the fits, T, τ_{in}, S, and τ_c varied, while the functions $C^{\alpha}_{2,\mathrm{FD}}(t)$ were completely fixed using the values of D_{xx}, D_{yy}, and D_{zz} from Section 3.4. The fits are greatly improved from those shown in Figure 12a, demonstrating the importance of including the ballistic and wobbling-in-a-cone reorientational dynamics of benzonitrile. The fit for the z direction, which is the only direction accessible experimentally, is almost indistinguishable from the simulated correlation function. The parameters for the fits in Figure 12b are given in Table 3.

Comparing the cone angles between the simulation and experiment (z direction only), it is seen that good agreement was obtained for the diffusive and total cone angles θ_c and θ_{total} (the total angle is obtained from the product $Q_{\mathrm{tot}} = TS$), respectively. However, the fit to the simulation overestimates the inertial cone angle, θ_{in}. This is not too surprising. The determination of θ_{in} involves extrapolation of the measured anisotropy to time zero, making it prone to larger errors than the remaining cone angles. The wobbling-in-a-cone correlation time, $\tau_c \sim 6$ ps, agrees well between the simulation and experiment. Note that the total extent of the decay due to ballistic and wobbling-in-a-cone reorientation is ~30%. This is found by taking the initial value of the normalized correlation function, that is 1, and subtracting the square of the total order parameter, $Q^2_{\mathrm{tot}} = (TS)^2$. Thus, FD makes up ~70%, or the majority, of the decay. In the experiments, FD made up ~76%

https://doi.org/10.1021/acs.jpcb.0c11148
J. Phys. Chem. B 2021, 125, 3163−3177

Table 3. Parameters for the Complete (including Ballistic, Wobbling-in-a-Cone, and FD Dynamics) Fit to $C_2(t)$[a]

axis	θ_{in} (deg)	θ_c (deg)	θ_{total} (deg)	τ_{in} (ps)	τ_c (ps)	τ_1 (ps)	τ_2 (ps)
x	14 ± 2	26 ± 1	30 ± 1	0.22 ± 0.08	1.1 ± 0.1	8.1	16.4
y	18.6 ± 0.5	25.1 ± 0.4	31.0 ± 0.4	0.25 ± 0.02	1.7 ± 0.1	8.1	16.4
z	17.4 ± 0.1	21.7 ± 0.1	27.6 ± 0.1	0.49 ± 0.01	5.9 ± 0.1	8.1	16.4
z (expt.)	5 ± 6	23 ± 4	24 ± 3		6 ± 2		13.1 ± 0.7

[a]The experimental data are reproduced with permission from Yamada et al., J. Phys. Chem. B **122**, 12147-12153 (2018). Copyright 2018 American Chemical Society.

of the decay. Only the single time constant, $\tau_\perp = 13.1 \pm 0.7$ ps could be determined from the FD regime of the measured anisotropy decay. However, from the simulations, we are able to determine the theoretically predicted FD correlation times, $\tau_1 = (6D + 2\Delta)^{-1} = 8.1$ ps and $\tau_2 = (6D - 2\Delta)^{-1} = 16.4$ ps and show that they provide a very good description of the simulated correlation functions $C^{\alpha}_{2,FD}(t)$.

Why is a single FD time constant observed experimentally when theoretical considerations predict two? The answer lies in the amplitudes. From eq 31 for $C^{z}_{2,FD}(t)$ and eq 33, the amplitude of τ_1 is given by $A_1=(TSa)^2/N^2 = 0.034$ and the amplitude of τ_2 is given by $A_2=(TSb)^2/N^2 = 0.664$ out of a total amplitude of 1. Therefore, $\tau_1 = 8.1$ ps constitutes only 3% of the decay. To make matters worse, this time constant is roughly equal to the wobbling-in-a-cone correlation time, $\tau_c \sim 6$ ps, making it more difficult to resolve. The decay in the FD regime is thus dominated by τ_2. The simulations indicate that D_{yy} can be different from D_{xx}, and $C^{z}_{2,FD}(t)$ can still appear to be single exponential. In the limit $D_{xx} = D_{yy} = D_\perp$, $C^{z}_{2,FD}(t)$ is exactly single exponential and $\tau_2 = \tau_\perp = 1/6D_\perp$. In light of these new results, $\tau_\perp$ from our previous measurements[14] should perhaps be interpreted as the more general correlation time τ_2, with the unequal diffusion coefficients in the x and y directions. This interpretation is supported by the reasonable correspondence between the measured value $\tau_\perp = 13.1 \pm 0.7$ ps and $\tau_2 = 16.4$ ps from the simulations. For comparison, the amplitudes of τ_1 and τ_2 for the x and y directions are $A_1 = 0.6005$, $A_2 = 0.0575$ and $A_1 = 0.3409$, $A_2 = 0.2923$, respectively. Therefore, the 8.1 ps component is dominant for the x direction, which explains why it is the fastest decay. Both components are similarly weighted in the y direction, making it discernably biexponential.

4. CONCLUDING REMARKS

We have presented an MD simulation study with comparison to experimental results of OPCs in liquid benzonitrile. The simulations are in quantitative agreement with PSPP and OKE measurements (Figure 4); the ability of the simulations to reproduce these two very different experimental observables as well as a number of other experimental observables demonstrates the accuracy of the simulations. The results confirm that collective reorientation dominates the long-time relaxation of the PA-TCF (OKE experiments). Further analysis demonstrated that collision-induced decay mechanisms contribute significantly to the short-time relaxation but are negligible at longer times (>20 ps). The large static OPC parameter, $g_2 = 1.95$, and non-unity value of the dynamic OPC parameter, $j_2 = 1.17$, show that strong OPCs are present in bulk benzonitrile. Structural analysis confirmed the presence of a pronounced antiparallel arrangement of neighboring molecules in the liquid. Well-defined peaks in the N−H rdfs demonstrated that significant Coulombic interactions are a key factor driving the formation of these antiparallel structures. The single-molecule rotational dynamics measured in the IR anisotropy experiments were shown to be complex, consisting of inertial, wobbling-in-a-cone, and anisotropic FD processes. The wobbling-in-a-cone model and FD theory for an asymmetric rotor were successfully used to explain the reorientational dynamics along the three principal axes of benzonitrile (Figure 12b).

MD simulations can be used to clarify the contributions of basic molecular motions to the complex observables of PSPP and OKE spectroscopy. The ability to reproduce both of these distinct observables is a stringent test of the simulations. The simulations can further provide a molecular scale picture of the dominant local structures influencing the time-dependent measurements. This MD study of single-molecule and collective benzonitrile molecular motions indicates a promising pathway for future investigations of complex liquid structures and dynamics, possibly including confined or heterogeneous systems, for example hydrogels.

■ ASSOCIATED CONTENT

Supporting Information

The Supporting Information is available free of charge at https://pubs.acs.org/doi/10.1021/acs.jpcb.0c11148.

Modified force field parameters for benzonitrile, dynamical properties of benzonitrile from the modified force field and from other classic force fields, liquid structure factor, rdfs from the modified force field and from other classic force fields, temperature-dependent self-diffusion coefficients, semi-log plot of the simulated and experimental OKE signals, single-exponential fit to the simulated OKE signal, plot of the second-order Legendre polynomial, single-exponential fit to the simulated $C_2(t)$, comparison of $\psi^{MM,s}(t)$ and $C_2(t)$, velocity autocorrelation function, and procedure for calculating the RMSD (PDF)

■ AUTHOR INFORMATION

Corresponding Author

Michael D. Fayer − *Department of Chemistry, Stanford University, Stanford, California 94305, United States;* orcid.org/0000-0002-0021-1815; Phone: (650) 723-4446; Email: fayer@stanford.edu

Authors

Maolin Sha − *Department of Physics and Materials Engineering, Hefei Normal University, Hefei 230061, China; Department of Chemistry, Stanford University, Stanford, California 94305, United States*

Steven A. Yamada − *Department of Chemistry, Stanford University, Stanford, California 94305, United States;* orcid.org/0000-0003-3171-1625

Complete contact information is available at:

https://pubs.acs.org/10.1021/acs.jpcb.0c11148

Author Contributions

[§]M.S. and S.A.Y. contributed equally to this work.

Notes

The authors declare no competing financial interest.

Data are available, including the Gromacs files, by contacting Professor Maolin Sha Department of Physics and Materials Engineering Hefei Normal University Hefei 230061 China (email: franksha@aliyun.com).

■ ACKNOWLEDGMENTS

This work was funded by the Division of Chemical Sciences, Geosciences, and Biosciences, Office of Basic Energy Sciences of the U.S. Department of Energy through grant no. DE-FG03-84ER13251 (S.A.Y. and M.D.F.). S.A.Y. gratefully acknowledges the support of a Stanford Graduate Fellowship. M.S. was supported by the Project of the Anhui Higher Education Top-notch Talent of China (grant no. gxgwfx2018066) and the Natural Science Foundation of the Anhui Higher Education Institutions of China (grant no. KJ2017A930). We thank Weizhong Zheng (East China University of Science and Technology) for helpful discussions and suggestions.

■ REFERENCES

(1) Mukamel, S. *Principles of Nonlinear Optical Spectroscopy*; Oxford University Press: New York, 1995.

(2) Hamm, P.; Zanni, M. T. *Concepts and Methods of 2D Infrared Spectroscopy*; Cambridge University Press: New York, 2011; p 286.

(3) Tokmakoff, A. Orientational correlation functions and polarization selectivity for nonlinear spectroscopy of isotropic media. I. Third order. *J. Chem. Phys.* **1996**, *105*, 1−12.

(4) Tan, H.-S.; Piletic, I. R.; Fayer, M. D. Polarization selective spectroscopy experiments: methodology and pitfalls. *J. Opt. Soc. Am. B* **2005**, *22*, 2009−2017.

(5) McMorrow, D.; Lotshaw, W. T.; Kenney-Wallace, G. A. Femtosecond optical Kerr studies on the origin of the nonlinear responses in simple liquids. *IEEE J. Quantum Electron.* **1988**, *24*, 443−454.

(6) Kwak, K.; Zheng, J.; Cang, H.; Fayer, M. D. Ultrafast Two-Dimensional Infrared Vibrational Echo Chemical Exchange Experiments and Theory. *J. Phys. Chem. B* **2006**, *110*, 19998−20013.

(7) Loughnane, B. J.; Farrer, R. A.; Scodinu, A.; Fourkas, J. T. Dynamics of a wetting liquid in nanopores: An optical Kerr effect study of the dynamics of acetonitrile confined in sol-gel glasses. *J. Chem. Phys.* **1999**, *111*, 5116−5123.

(8) Fecko, C. J.; Eaves, J. D.; Tokmakoff, A. Isotropic and anisotropic Raman scattering from molecular liquids measured by spatially masked optical Kerr effect spectroscopy. *J. Chem. Phys.* **2002**, *117*, 1139−1154.

(9) Rezus, Y. L. A.; Bakker, H. J. On the Orientational Relaxation of HDO in Liquid Water. *J. Chem. Phys.* **2005**, *123*, 114502.

(10) Zheng, J.; Kwak, K.; Asbury, J.; Chen, X.; Piletic, I. R.; Fayer, M. D. Ultrafast Dynamics of Solute-Solvent Complexation Observed at Thermal Equilibrium in Real Time. *Science* **2005**, *309*, 1338.

(11) Perakis, F.; Hamm, P. Two-Dimensional Infrared Spectroscopy of Supercooled Water. *J. Phys. Chem. B* **2011**, *115*, 5289−5293.

(12) Ren, Z.; Brinzer, T.; Dutta, S.; Garrett-Roe, S. Thiocyanate as a Local Probe of Ultrafast Structure and Dynamics in Imidazolium-Based Ionic Liquids: Water-Induced Heterogeneity and Cation-Induced Ion Pairing. *J. Phys. Chem. B* **2015**, *119*, 4699−4712.

(13) Hoffman, D. J.; Fayer, M. D. Discontinuity in Fast Dynamics at the Glass Transition of ortho-Terphenyl. *J. Phys. Chem. B* **2017**, *121*, 10417−10428.

(14) Yamada, S. A.; Bailey, H. E.; Fayer, M. D. Orientational Pair Correlations in a Dipolar Molecular Liquid: Time-Resolved Resonant and Nonresonant Pump-Probe Spectroscopies. *J. Phys. Chem. B* **2018**, *122*, 12147−12153.

(15) Kinoshita, S.; Sakai, Y.; Miyazaki, J.; Watanabe, J. Fundamental aspects of light scattering and optical Kerr effect spectroscopy. *Eur. Phys. J.: Spec. Top.* **2012**, *209*, 1−100.

(16) Righini, R. Ultrafast Optical Kerr Effect in Liquids and Solids. *Science* **1993**, *262*, 1386−1390.

(17) Bartolini, P.; Taschin, A.; Eramo, R.; Torre, R. Optical Kerr Effect Experiments on Complex Liquids. In *Time-Resolved Spectroscopy in Complex Liquids: An Experimental Perspective*; Torre, R., Ed.; Springer: New York, 2008.

(18) Tao, T. Time-dependent fluorescence depolarization and Brownian rotational diffusion coefficients of macromolecules. *Biopolymers* **1969**, *8*, 609−632.

(19) Boyd, R. W. *Nonlinear Optics*, 3rd ed.; Academic Press: New York, 2008.

(20) Hellwarth, R. W. Third-order optical susceptibilities of liquids and solids. *Prog. Quantum Electron.* **1977**, *5*, 1−68.

(21) Whittenburg, S. L.; Wang, C. H. Light scattering studies of transverse sound wave and molecular motion in benzonitrile. *J. Chem. Phys.* **1977**, *66*, 4995−5000.

(22) Bertucci, S. J.; Burnham, A. K.; Alms, G. R.; Flygare, W. H. Light scattering studies of orientational pair correlations in liquids composed of anisometric molecules. *J. Chem. Phys.* **1977**, *66*, 605−616.

(23) Alms, G. R.; Patterson, G. D. Depolarized Rayleigh scattering from benzonitrile. *J. Chem. Phys.* **1978**, *68*, 3440−3444.

(24) Whittenburg, S. L.; Wang, C. H. Comment on "Depolarized Rayleigh spectroscopy from benzonitrile". *J. Chem. Phys.* **1979**, *71*, 561−562.

(25) Kivelson, D.; Madden, P. A. Light Scattering Studies of Molecular Liquids. *Annu. Rev. Phys. Chem.* **1980**, *31*, 523−558.

(26) Guillaume, F.; Yarwood, J.; Price, A. H. Infrared, Raman and microwave studies of the molecular dynamics and interactions in liquid benzonitrile. *Mol. Phys.* **1987**, *62*, 1307−1321.

(27) Smith, N. A.; Meech, S. R. Ultrafast Dynamics of Polar Monosubstituted Benzene Liquids Studied by the Femtosecond Optical Kerr Effect. *J. Phys. Chem. A* **2000**, *104*, 4223−4235.

(28) Ladanyi, B. M.; Liang, Y. Q. Interaction-induced contributions to polarizability anisotropy relaxation in polar liquids. *J. Chem. Phys.* **1995**, *103*, 6325−6332.

(29) Milischuk, A. A.; Ladanyi, B. M. Polarizability Anisotropy Relaxation in Nanoconfinement: Molecular Simulation Study of Acetonitrile in Silica Pores. *J. Phys. Chem. B* **2013**, *117*, 15729−15740.

(30) Lipari, G.; Szabo, A. Effect of librational motion on fluorescence depolarization and nuclear magnetic resonance relaxation in macromolecules and membranes. *Biophys. J.* **1980**, *30*, 489−506.

(31) Lipari, G.; Szabo, A. Model-free approach to the interpretation of nuclear magnetic resonance relaxation in macromolecules. 1. Theory and range of validity. *J. Am. Chem. Soc.* **1982**, *104*, 4546−4559.

(32) Tan, H.-S.; Piletic, I. R.; Fayer, M. D. Orientational dynamics of water confined on a nanometer length scale in reverse micelles. *J. Chem. Phys.* **2005**, *122*, 174501.

(33) Frenkel, D.; McTague, J. P. Molecular dynamics studies of orientational and collision-induced light scattering in molecular fluids. *J. Chem. Phys.* **1980**, *72*, 2801−2818.

(34) Paolantoni, M.; Ladanyi, B. M. Polarizability anisotropy relaxation in liquid ethanol: A molecular dynamics study. *J. Chem. Phys.* **2002**, *117*, 3856−3873.

(35) Elola, M. D.; Ladanyi, B. M. Polarizability response in polar solvents: Molecular-dynamics simulations of acetonitrile and chloroform. *J. Chem. Phys.* **2005**, *122*, 224506.

(36) Elola, M. D.; Ladanyi, B. M. Molecular Dynamics Study of Polarizability Anisotropy Relaxation in Aromatic Liquids and Its Connection with Local Structure. *J. Phys. Chem. B* **2006**, *110*, 15525−15541.

(37) Milischuk, A. A.; Ladanyi, B. M. Polarizability anisotropy relaxation in nanoconfinement: Molecular simulation study of water in cylindrical silica pores. *J. Chem. Phys.* **2014**, *141*, 18C513.
(38) Riddick, J. A.; Bunger, W. B.; Sakano, T. K. *Organic Solvents: Physical Properties and Methods of Purification*, 4th ed.; John Wiley and Sons: New York, NY, United States, 1986.
(39) Zare, R. N. *Angular Momentum: Understanding Spatial Aspects in Chemistry and Physics*; John Wiley & Sons: New York, 1988.
(40) Berne, B. J.; Pecora, R. *Dynamic Light Scattering: With Applications to Chemistry, Biology, and Physics*; Dover: New York, 2000.
(41) Abdoul-Carime, H.; Desfrançois, C. Electrons weakly bound to molecules by dipolar, quadrupolar or polarization forces. *Eur. Phys. J. D* **1998**, *2*, 149−156.
(42) Frisch, M. J.; Trucks, G. W.; Schlegel, H. B.; Scuseria, G. E.; Robb, M. A.; Cheeseman, J. R.; Montgomery, J. A.; Vreven, T.; Kudin, K. N.; Burant, J. C.; Millam, J. M.; Iyengar, S. S.; Tomasi, J.; Barone, V.; Mennucci, B.; Cossi, M.; Scalmani, G.; Rega, N.; Petersson, G. A.; Nakatsuji, H.; Hada, M.; Ehara, M.; Toyota, K.; Fukuda, R.; Hasegawa, J.; Ishida, M.; Nakajima, T.; Honda, Y.; Kitao, O.; Nakai, H.; Klene, M.; Li, X.; Knox, J. E.; Hratchian, H. P.; Cross, J. B.; Bakken, V.; Adamo, C.; Jaramillo, J.; Gomperts, R.; Stratmann, R. E.; Yazyev, O.; Austin, A. J.; Cammi, R.; Pomelli, C.; Ochterski, J. W.; Ayala, P. Y.; Morokuma, K.; Voth, G. A.; Salvador, P.; Dannenberg, J. J.; Zakrzewski, V. G.; Dapprich, S.; Daniels, A. D.; Strain, M. C.; Farkas, O.; Malick, D. K.; Rabuck, A. D.; Raghavachari, K.; Foresman, J. B.; Ortiz, J. V.; Cui, Q.; Baboul, A. G.; Clifford, S.; Cioslowski, J.; Stefanov, B. B.; Liu, G.; Liashenko, A.; Piskorz, P.; Komaromi, I.; Martin, R. L.; Fox, D. J.; Keith, T.; Al-Laham, M. A.; Peng, C. Y.; Nanayakkara, A.; Challacombe, M.; Gill, P. M. W.; Johnson, B.; Chen, W.; Wong, M. W.; Gonzalez, C.; Pople, J. A. *Gaussian 03*, Revision C. 02; Gaussian Inc.: Wallingford, CT, 2004.
(43) Jorgensen, W. L.; Laird, E. R.; Nguyen, T. B.; Tirado-Rives, J. Monte Carlo simulations of pure liquid substituted benzenes with OPLS potential functions. *J. Comput. Chem.* **1993**, *14*, 206−215.
(44) Lemkul, J. From proteins to perturbed Hamiltonians: A suite of tutorials for the GROMACS-2018 molecular simulation package [article v1. 0]. *Living J. Comp. Mol. Sci.* **2018**, *1*, 5068.
(45) Loubet, B.; Kopec, W.; Khandelia, H. Accelerating All-Atom MD Simulations of Lipids Using a Modified Virtual-Sites Technique. *J. Chem. Theory Comput.* **2014**, *10*, 5690−5695.
(46) Lavino, A. D.; Banetta, L.; Carbone, P.; Marchisio, D. L. Extended Charge-On-Particle Optimized Potentials for Liquid Simulation Acetone Model: The Case of Acetone-Water Mixtures. *J. Phys. Chem. B* **2018**, *122*, 5234−5241.
(47) Deng, M.; Shen, H. Coarse-Grained Model for Water Involving a Virtual Site. *J. Phys. Chem. B* **2016**, *120*, 733−739.
(48) Wang, J.; Wolf, R. M.; Caldwell, J. W.; Kollman, P. A.; Case, D. A. Development and testing of a general amber force field. *J. Comput. Chem.* **2004**, *25*, 1157−1174.
(49) Vanommeslaeghe, K.; Hatcher, E.; Acharya, C.; Kundu, S.; Zhong, S.; Shim, J.; Darian, E.; Guvench, O.; Lopes, P.; Vorobyov, I.; Mackerell, A. D., Jr. CHARMM general force field: A force field for drug-like molecules compatible with the CHARMM all-atom additive biological force fields. *J. Comput. Chem.* **2010**, *31*, 671−690.
(50) Van Der Spoel, D.; Lindahl, E.; Hess, B.; Groenhof, G.; Mark, A. E.; Berendsen, H. J. C. GROMACS: fast, flexible, and free. *J. Comput. Chem.* **2005**, *26*, 1701−1718.
(51) Abraham, M. J.; Murtola, T.; Schulz, R.; Páll, S.; Smith, J. C.; Hess, B.; Lindahl, E. GROMACS: High performance molecular simulations through multi-level parallelism from laptops to supercomputers. *SoftwareX* **2015**, *1−2*, 19−25.
(52) Maitland, G. C.; Rigby, M.; Smith, E. B.; Wakeham, W. A. *Intermolecular Forces: Their Origin and Determination*; Clarendon Press: Oxford, 1981.
(53) Hess, B.; Bekker, H.; Berendsen, H. J. C.; Fraaije, J. G. E. M. LINCS: A linear constraint solver for molecular simulations. *J. Comput. Chem.* **1997**, *18*, 1463−1472.
(54) Darden, T.; York, D.; Pedersen, L. Particle mesh Ewald: AnN·log(N) method for Ewald sums in large systems. *J. Chem. Phys.* **1993**, *98*, 10089−10092.
(55) Berendsen, H. J. C.; Postma, J. P. M.; van Gunsteren, W. F.; DiNola, A.; Haak, J. R. Molecular dynamics with coupling to an external bath. *J. Chem. Phys.* **1984**, *81*, 3684−3690.
(56) Bussi, G.; Donadio, D.; Parrinello, M. Canonical sampling through velocity rescaling. *J. Chem. Phys.* **2007**, *126*, 014101.
(57) Viswanathan, S.; Anand Rao, M.; Prasad, D. H. L. Densities and Viscosities of Binary Liquid Mixtures of Anisole or Methyltert-Butyl Ether with Benzene, Chlorobenzene, Benzonitrile, and Nitrobenzene. *J. Chem. Eng. Data* **2000**, *45*, 764−770.
(58) Lei, Y.; Chen, Z.; An, X.; Huang, M.; Shen, W. Measurements of Density and Heat Capacity for Binary Mixtures {x Benzonitrile + (1 −x) (Octane or Nonane)}. *J. Chem. Eng. Data* **2010**, *55*, 4154−4161.
(59) Nikam, P. S.; Kharat, S. J. Excess Molar Volumes and Deviations in Viscosity of Binary Mixtures ofN,N-Dimethylformamide with Aniline and Benzonitrile at (298.15, 303.15, 308.15, and 313.15) K. *J. Chem. Eng. Data* **2003**, *48*, 972−976.
(60) Abraham, R.; Abdulkhadar, M.; Asokan, C. V. Ultrasonic investigation of molecular interaction in binary mixtures of nitriles with methanol/toluene. *J. Chem. Thermodyn.* **2000**, *32*, 1−16.
(61) Katayama, M.; Komori, K.; Ozutsumi, K.; Ohtaki, H. The Liquid Structure of Various Nitriles andN,N-Dimethylformamide Studied by the X-Ray Diffraction Method Using a CCD Detector. *Z. Phys. Chem.* **2004**, *218*, 659.
(62) McMorrow, D.; Lotshaw, W. T. Intermolecular dynamics in acetonitrile probed with femtosecond Fourier-transform Raman spectroscopy. *J. Phys. Chem.* **1991**, *95*, 10395−10406.
(63) Loughnane, B. J.; Farrer, R. A.; Fourkas, J. T. Evidence for the Direct Observation of Molecular Exchange of a Liquid at the Solid/Liquid Interface. *J. Phys. Chem. B* **1998**, *102*, 5409−5412.
(64) McMorrow, D.; Lotshaw, W. T. Evidence for low-frequency (≈ 15 cm−1) collective modes in benzene and pyridine liquids. *Chem. Phys. Lett.* **1993**, *201*, 369−376.
(65) Cong, P.; Deuel, H. P.; Simon, J. D. Structure and dynamics of molecular liquids investigated by optical-heterodyne detected Raman-induced Kerr effect spectroscopy (OHD-RIKES). *Chem. Phys. Lett.* **1995**, *240*, 72−78.
(66) Neelakandan, M.; Pant, D.; Quitevis, E. L. Reorientational and intermolecular dynamics in binary liquid mixtures of hexafluorobenzene and benzene: femtosecond optical Kerr effect measurements. *Chem. Phys. Lett.* **1997**, *265*, 283−292.
(67) Fayer, M. D. Dynamics and structure of room temperature ionic liquids. *Chem. Phys. Lett.* **2014**, *616−617*, 259−274.
(68) Keyes, T.; Kivelson, D. Depolarized Light Scattering: Theory of the Sharp and Broad Rayleigh Lines. *J. Chem. Phys.* **1972**, *56*, 1057−1065.
(69) Keyes, T. Microscopic theory of collective anisotropic molecular reorientation. *Mol. Phys.* **1972**, *23*, 737−743.
(70) Alms, G. R.; Bauer, D. R.; Brauman, J. I.; Pecora, R. Depolarized Rayleigh scattering and orientational relaxation of molecules in solution. II Chloroform and nitrobenzene. *J. Chem. Phys.* **1973**, *59*, 5310−5320.
(71) Versmold, H. Depolarized Rayleigh Scattering: Reorientational Motion and Orientational Correlations in Acetonitrile and Carbon Disulfide. *Ber. Bunsenges. Phys. Chem.* **1978**, *82*, 451−457.
(72) Gierke, T. D. Dynamic orientational pair correlations in symmetric tops and static orientational pair correlations in anisometric molecules. *J. Chem. Phys.* **1976**, *65*, 3873−3882.
(73) Bauer, D. R.; Brauman, J. I.; Pecora, R. Depolarized light scattering from liquids. *Annu. Rev. Phys. Chem.* **1976**, *27*, 443−463.
(74) Shikata, T.; Sugimoto, N.; Sakai, Y.; Watanabe, J. Dielectric Behaviors of Typical Benzene Monosubstitutes, Bromobenzene and Benzonitrile. *J. Phys. Chem. B* **2012**, *116*, 12605−12613.
(75) Hsu, C. S.; Chandler, D. RISM calculation of the structure of liquid acetonitrile. *Mol. Phys.* **1978**, *36*, 215−224.
(76) Mazza, M. G.; Giovambattista, N.; Stanley, H. E.; Starr, F. W. Connection of translational and rotational dynamical heterogeneities

https://doi.org/10.1021/acs.jpcb.0c11148
J. Phys. Chem. B 2021, 125, 3163−3177

with the breakdown of the Stokes-Einstein and Stokes-Einstein-Debye relations in water. *Phys. Rev. E: Stat., Nonlinear, Soft Matter Phys.* **2007**, *76*, 031203.
(77) Favro, L. D. Theory of the Rotational Brownian Motion of a Free Rigid Body. *Phys. Rev.* **1960**, *119*, 53−62.
(78) Huntress, W. T., Jr. Effects of Anisotropic Molecular Rotational Diffusion on Nuclear Magnetic Relaxation in Liquids. *J. Chem. Phys.* **1968**, *48*, 3524−3533.
(79) Huntress, W. T. The Study of Anisotropic Rotation of Molecules in Liquids by NMR Quadrupolar Relaxation. In *Advances in Magnetic and Optical Resonance*; Waugh, J. S., Ed.; Academic Press, 1970; Vol. *4*, pp 1−37.
(80) Chuang, T. J.; Eisenthal, K. B. Theory of Fluorescence Depolarization by Anisotropic Rotational Diffusion. *J. Chem. Phys.* **1972**, *57*, 5094−5097.
(81) Ehrenberg, M.; Rigler, R. Polarized fluorescence and rotational brownian motion. *Chem. Phys. Lett.* **1972**, *14*, 539−544.
(82) Kinosita, K.; Kawato, S.; Ikegami, A. A theory of fluorescence polarization decay in membranes. *Biophys. J.* **1977**, *20*, 289−305.
(83) Gordon, R. G. Molecular Motion in Infrared and Raman Spectra. *J. Chem. Phys.* **1965**, *43*, 1307−1312.
(84) Cox, J. D.; Pilcher, G. *Thermochemistry of Organic and Organometallic Compounds*; Academic Press, New York, 1970.

https://doi.org/10.1021/acs.jpcb.0c11148
J. Phys. Chem. B 2021, 125, 3163−3177